

## Supporting Information

### **The origin of stability and high $\text{Co}^{3+/2+}$ redox utilization for $\text{FePO}_4$ -coated $\text{LiCo}_{0.90}\text{Ti}_{0.05}\text{PO}_4$ / MWCNT nanocomposites for 5 V class lithium ion batteries**

Naohisa Okita<sup>1,2</sup>, Etsuro Iwama<sup>1,2,3</sup>, Yusuke Takami<sup>1</sup>, Shingo Abo<sup>1</sup>, Wako Naoi<sup>3,4</sup>, Patrick Rozier<sup>2,5,6</sup>, Patrice Simon<sup>2,5,6</sup>, McMahon Thomas Homer Reid<sup>2,3,7</sup>, and Katsuhiko Naoi<sup>1,2,3\*</sup>

<sup>1</sup>*Department of Applied Chemistry, Tokyo University of Agriculture & Technology, 2-24-16 Naka-cho, Koganei, Tokyo 184-8588, Japan*

<sup>2</sup>*Global Innovation Research Organization, Tokyo University of Agriculture & Technology, 2-24-16 Naka-cho, Koganei, Tokyo, 184-8588 Japan*

<sup>3</sup>*Advanced Capacitor Research Center, Tokyo University of Agriculture & Technology, 2-24-16 Naka-cho, Koganei, Tokyo 184-8588, Japan*

<sup>4</sup>*Division of Art and Innovative Technologies, K & W Inc., 1-3-16-901 Higashi, Kunitachi, Tokyo 186-0002, Japan*

<sup>5</sup>*Réseau sur le Stockage Electrochimique de l'Energie (RS2E), France CNRS 3459*

<sup>6</sup>*CIRIMAT, Université de Toulouse, CNRS, Université Toulouse 3 - Paul Sabatier, 118 Route de Narbonne, 31062 Toulouse cedex 9 - France.*

<sup>7</sup>*Simpetus LLC., 1 Fitchburg St, Somerville, MA 02143, USA*

\* E-mail: n-okita@go.tuat.ac.jp / iwama@cc.tuat.ac.jp / k-naoi@cc.tuat.ac.jp

### The carbon content in the resultant material

The thermogravimetric/differential thermal analyzer (TG/DTA) curves of the  $\text{LiCoPO}_4$  (LCP)/Multiwalled carbon nanotube (MWCNT),  $\text{LiCo}_{0.9}\text{Ti}_{0.05}\text{PO}_4$  (LCTP)/MWCNT, and  $\text{FePO}_4$  (FP)-coated LCTP/MWCNT are shown in Figure S1. The calculated weight ratios of MWCNT in composites—LCP/MWCNT, LCTP/MWCNT, and FP-coated LCTP/MWCNT—were 27, 30, 25 wt.%, respectively.

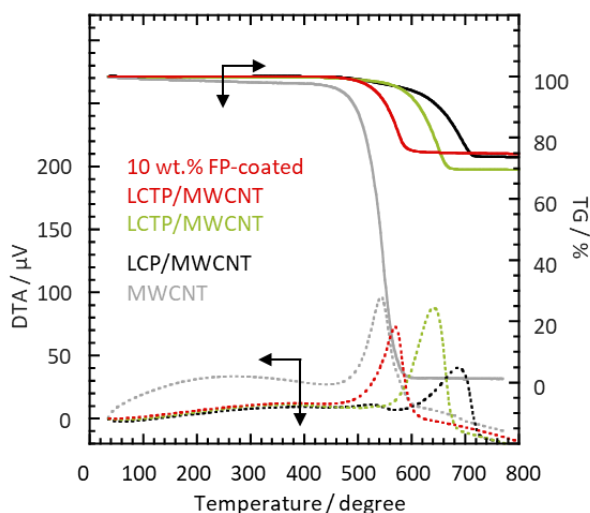


Figure S1 TG/DTA curves for LCP/MWCNT, LCTP/MWCNT, and FP-coated LCTP/MWCNT.

### Comparison of different aliovalent substitution

To further improve electrochemical characteristic of previously-reported  $\text{LiCo}_{0.8}\text{Fe}_{0.2}\text{PO}_4$  (LCFP), we consider Ti dopant yielding the aliovalent-substituted LCP variants  $\text{LiCo}_{1-2x}\text{Ti}_x\text{PO}_4$  (referred to below as LCTP)—because Ti is multivalent element which can exist at valence states equal to or higher than that of  $\text{Fe}^{3+}$ , allowing creation of vacancies in the bulk LCP crystal. Considering the valence states of Ti as 4+, we synthesized LCTP composites with a substitution concentration  $x = 3, 5, 7, \text{ and } 10$  at.%. We fabricated cells with cathodes made from synthesized composites and compared their initial discharge capacity (Figure S2a). Among them, the 5 at.% of Ti-substitution was the optimum value, as the electrochemical signal of impurity phase  $\text{LiTi}_2(\text{PO}_4)_3$  (LTP) can be detected with  $x > 5$  at.% in LCTP as shown in Figure S2a. We also found that LCTP surpassed  $\text{V}^{3+}$ -substituted LCP, LCFP, and LCP in terms of discharge capacity. (Figure S2b)

The observed overpotential in the discharge curve for  $\text{LiCo}_{0.9}\text{Ti}_{0.05}\text{PO}_4$  (LCTP)/MWCNT was higher than that for LCP/MWCNT and LCFP/MWCNT, as shown in Figure S2b. To understand the reason behind of such high overpotential, we have conducted the electrochemical impedance spectroscopy (EIS) measurements at SOC = 0 and 70 % on several LCP-derive composites including LCTP/MWCNT. As shown in Figure S3a, the EIS spectra for the LCTP/MWCNT at SOC = 0 % showed a large semicircle (*ca.*  $180 \Omega \text{ cm}^2$ ) at middle frequency around 20 Hz compared to other two samples. Such large semicircle may be due to the minute presence of impurity phase such as  $\text{LiTi}_2(\text{PO}_4)_3$  (LTP), which was more clearly detected in electrochemical signals with an increase of Ti content  $> 5$  at.% as shown in Figure S2a. At SOC = 70% (see Figure S3b), the semicircle for the became larger ( $650 \Omega \text{ cm}^2$ ) because of the overlapped charge transfer resistance ( $R_{ct}$ ). The appeared semicircle for the LCTP/MWCNT was the largest among three samples, which well corresponds to the observed largest overpotential in discharge curve. Again, such large  $R_{ct}$  can be attributed to the possible existence of LTP phase.

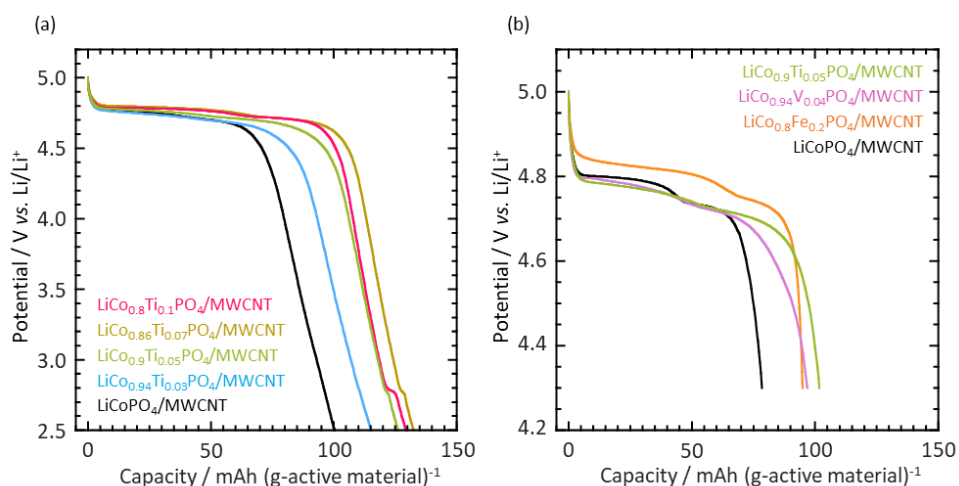


Figure S2 (a) Discharge curves of  $x$  wt.% ( $x = 3, 5, 7,$  and  $10$ )  $\text{Ti}^{4+}$ -substituted LCP/MWCNT composites. Confined operation voltage: 2.5-5.0 V vs. Li was applied. (b) Discharge curves of  $\text{M}^{n+}$  ( $\text{M}^{n+} = \text{Ti}^{4+}, \text{V}^{3+},$  and  $\text{Fe}^{3+}$ )-substituted LCP/MWCNT composites Confined operation voltage: 4.3-5.0 V vs. Li was applied.

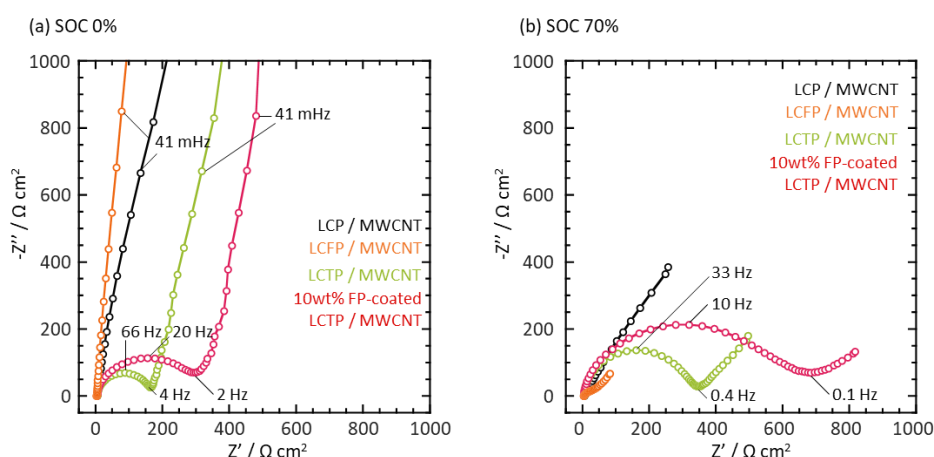


Figure S3 EIS spectra for LCP /MWCNT, LCFP/MWCNT, LCTP/MWCNT, and FP-coated LCTP/MWCNT (a) at SOC = 0 and (b)70 %.

Enlarged X-ray diffraction (XRD) patterns of uncoated LCP, uncoated LCTP, and FP-coated LCTP

Enlarged X-ray diffraction (XRD) patterns of all three samples (uncoated LCP, uncoated LCTP, and FP-coated LCTP) were recorded in Figure S4. In the solid solution domain, the positions of some Bragg peaks were shifted by Ti-substitution or FP-coating.

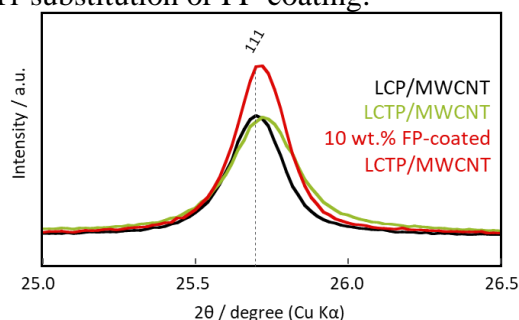


Figure S4 Enlarged XRD patterns of uncoated LCP, uncoated LCTP, and FP-coated LCTP.

### Surface composition change with aliovalent substitution and FP-coating

To investigate the surface composition of four compounds, X-ray photoelectron spectroscopy (XPS) analyses of Co  $2p_{3/2}$ , Ti  $2p_{3/2}$ , and Fe  $2p_{3/2}$  were performed on the LCTP particles with or without FP-coating, subjected to different Ar ion etching duration. The change in peak intensity with etching times differs depending on the atom species (Co, Fe, or Ti, see Figure S5), indicating the difference of composition ratio between surface (pristine) and the inner bulk (after etching up to 30 sec). The Co/Ti, Co/Fe, and Co/Ti/Fe ratios were calculated by computing the areas under the Co  $2p_{3/2}$ , Ti  $2p_{3/2}$ , and Fe  $2p_{3/2}$  peaks and reported in the Figure 3. Examination of the results for LCTP particles shows that the distribution of Co and Ti at the surface (Co/Ti = 88/12) only slightly differs from that in the bulk (Co/Ti = 93/7). Differently, the FP-coating drastically changes the surface composition (Co/Ti/Fe = 50/15/35) from the bulk composition (Co/Ti/Fe = 62/10/28), indicating the successful formation of an Fe<sup>3+</sup>-rich phase on the LCTP surface, as we previously reported for LCFP and FP-coated LCP<sup>1-2</sup>. In the survey spectra for three samples (Figure S6), no clear peaks corresponding to impurities were found for the pristine composites apart from the cathode compositions, including Co, Fe, Ti, Li, P, O, C (mainly MWCNT) and F (PVdF binder)-based compounds.

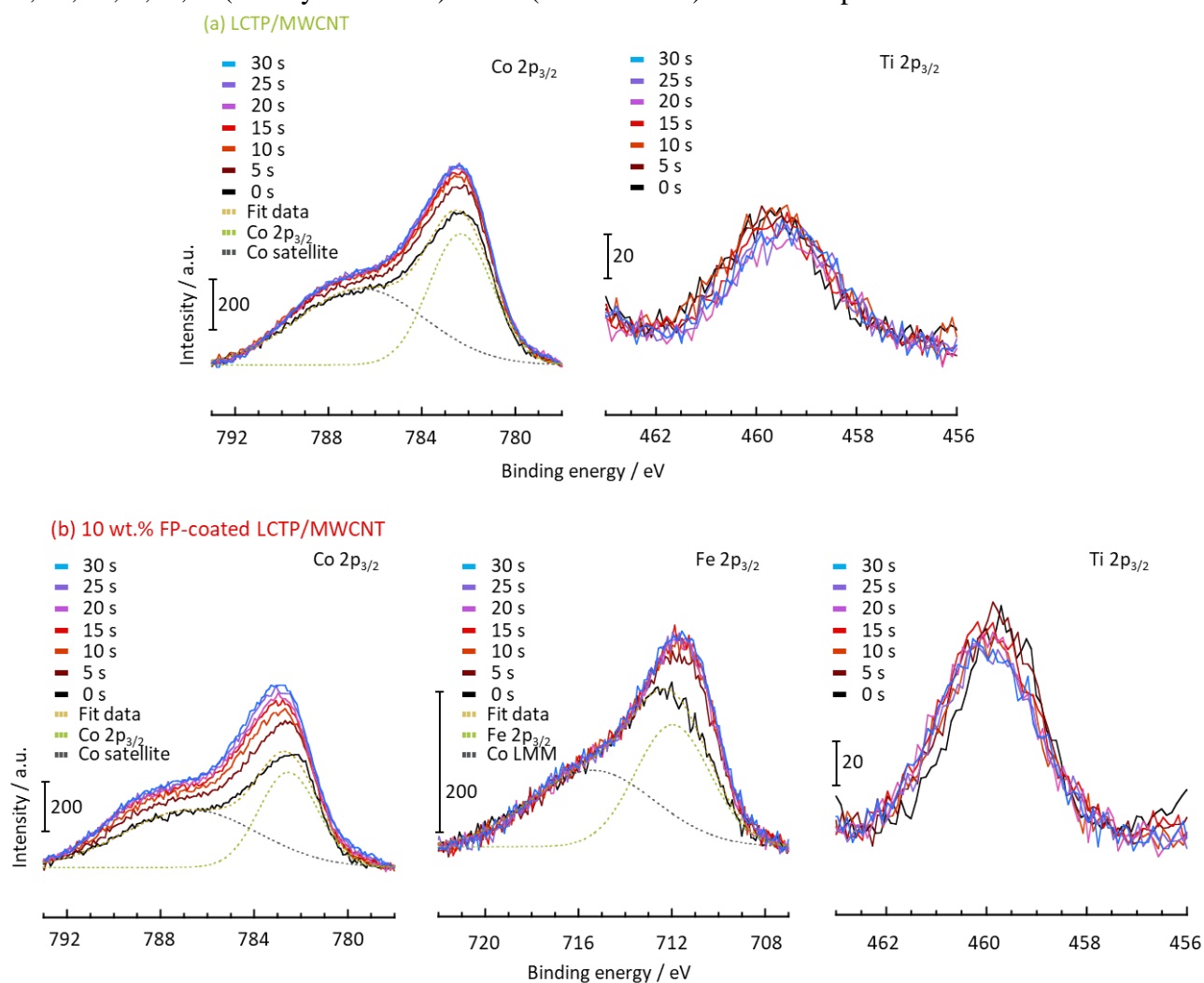


Figure S5 Consecutive XPS measurements with data acquisition at 5 s intervals during 0–30 s Ar ion etching. Depth profiles of Co, Fe, and Ti for (a) LCTP and (b) FP-coated LCTP / MWCNT composites.

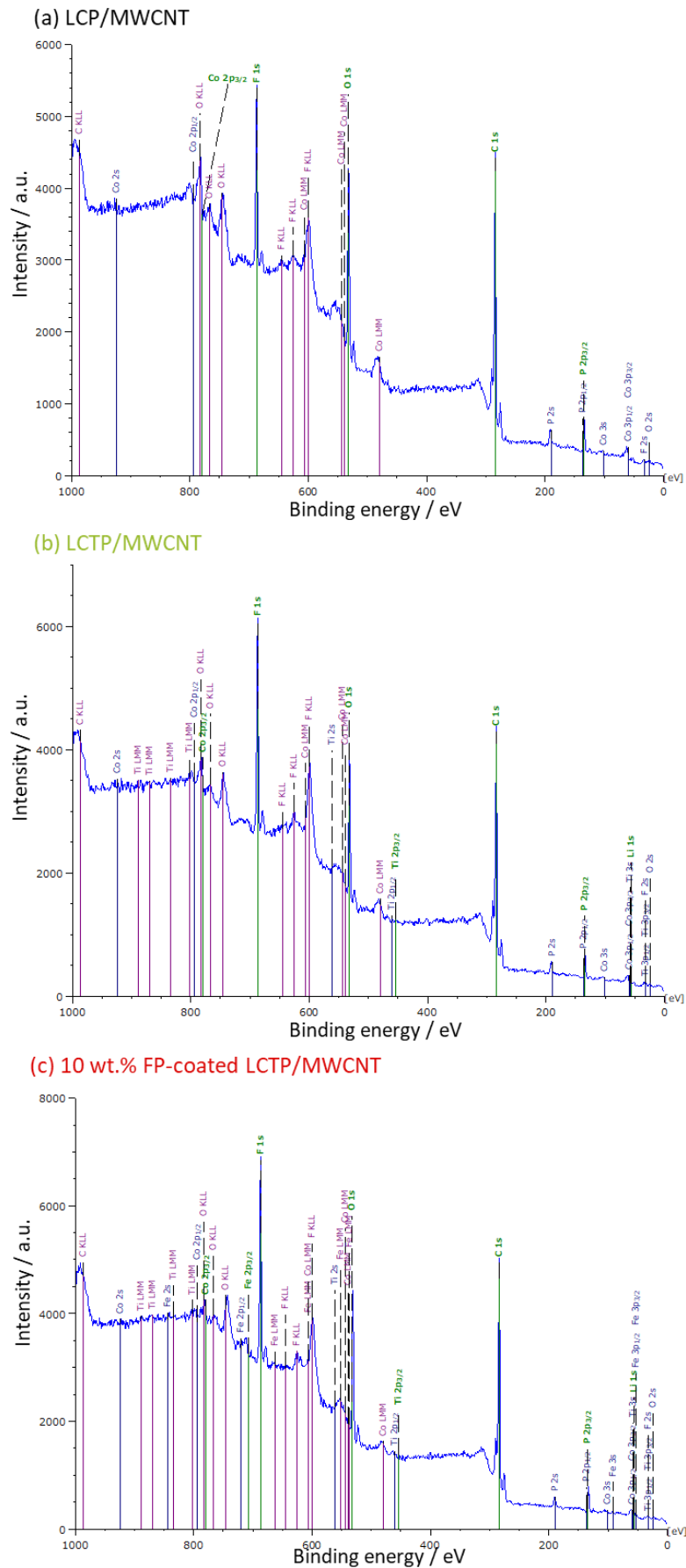


Figure S6 Survey spectra of (a) LCP, (b) LCTP and (c) FP-coated LCTP / MWCNT composites.

### X-ray absorption fine structure (XANES) of Co, Fe, and Ti K-edge.

To see the effect of FP-coating and Ti-substitution on the redox state of Co, Fe and Ti, *in situ* XAFS measurements were conducted for the four different samples at 1<sup>st</sup> and 50<sup>th</sup> cycle. The X-ray absorption near edge structure (XANES) spectra of Co, Fe and Ti K-edge for the LCP/MWCNT or LCTP/MWCNT composites with or without FP-coating are shown in Figure S7. Different Co valence states are determined for the three as-prepared electrodes, where those in LCTP samples correspond to Co = +2 regardless of FP-coating, while LCP sample show Co = +2.13. The difference of Co valence states between uncoated LCP and LCTP, which equals to 0.13, cannot be simply explained by the different amounts of Co<sub>3</sub>O<sub>4</sub> (average valence state Co = +2.66) impurity phase evaluated from the XRD patterns fitting (10%, see Table 2). Although the explanation of such difference is still unspecified, a role of Ti and generated vacancies can be suggested to favor the stabilization of Co in electrochemically active +2 valence state leading to increased capacity compared to samples which contain some Co in inactive +3 valence state. During the first cycle, at the charged state, the Co valence state increases, and reaches much higher value for FP-coated sample (+2.82) compared to uncoated one (+2.66). The comparison of the Co valence state at charged state along cycles shows that after 50 cycles FP-coated samples are stable while uncoated ones shows a clear decrease in agreement with already discussed capacity retention capabilities.

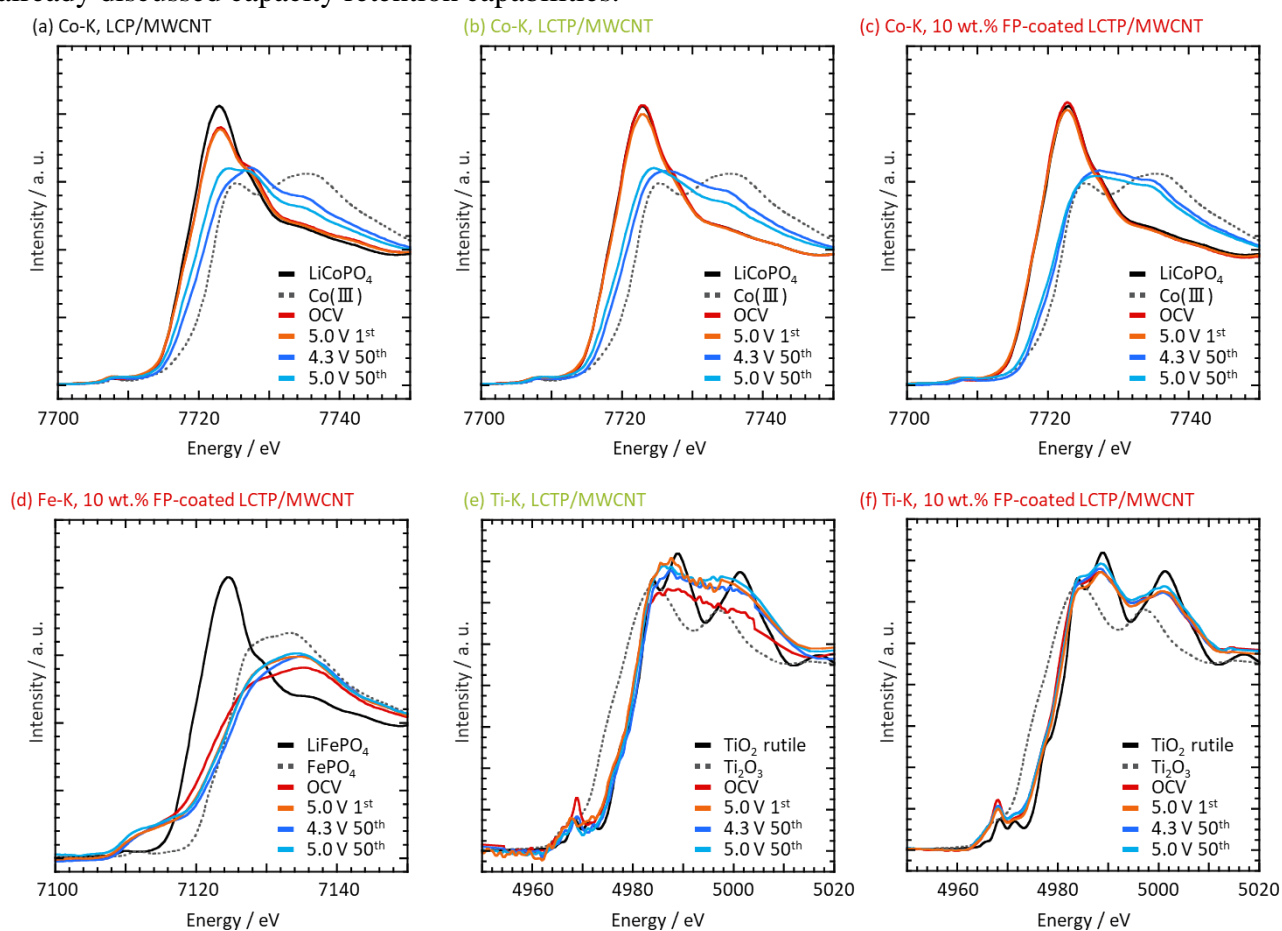


Figure S7 Co-K XANES spectra for (a) LCP, (b) LCTP, and (c) FP-coated LCTP/MWCNT composites. Fe-K XANES spectra for (d) FP-coated LCTP/MWCNT composites. Ti-K XANES spectra for (e) LCTP and (f) FP-coated LCTP/MWCNT composites.

### Electrochemical characterization via GITT measurements

To investigate electrochemical kinetics and stability, galvanostatic intermittent titration technique (GITT) measurements for all three samples—uncoated LCP, uncoated LCTP, and FP-coated LCTP—were performed. As shown in Figure S8a, GITT charge curve for LCP shows typical two plateau regions. The observed large polarization—particularly in the 2<sup>nd</sup> plateau at 4.8 V vs. Li—suggests slow kinetics of Li deintercalation in LCP, while the corresponding irreversible change in capacity suggests instability of the delithiated phase. Meanwhile, the polarization observed for uncoated LCTP—which contains 5 at.% Ti incorporated into LCP—are as large as the uncoated LCP (Figure S8b). In contrast, the dramatic decrease in polarizability was observed for FP-coated LCTP shown in Figure S8c. This indicates that the surface Fe<sup>3+</sup> enrichment brings about the stability enhancement of the delithiated phase, leading to excellent long term cyclability, while Ti<sup>4+</sup>-substitution contributes to the higher utilization of Co in LCTP crystals.

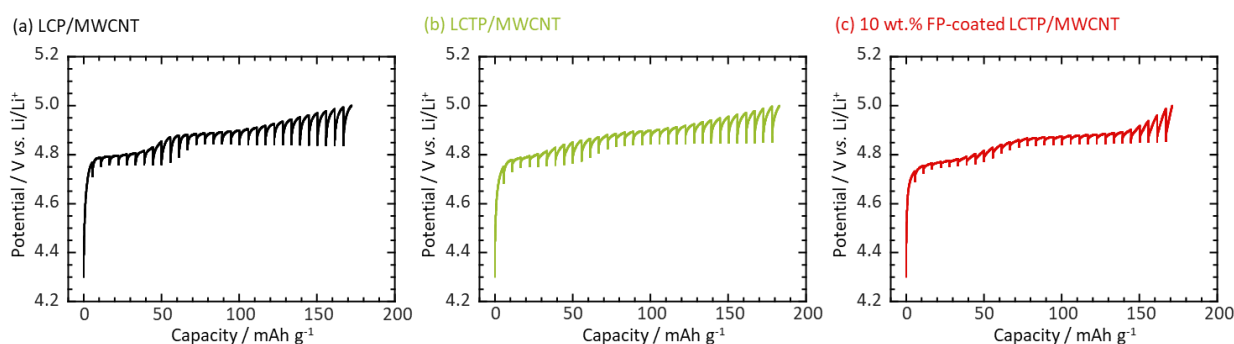


Figure S8 GITT polarization curves for (a) LCP, (b) LCTP, and (c) FP-coated LCTP. GITT was conducted with 0.1C (1C = 167 mAh g<sup>-1</sup> per active material) for 20 min. and rest time for 1h in the potential range of between 4.3-5.0 V vs. Li/Li<sup>+</sup>. Before GITT measurements, a pre-cycling was conducted at 0.1C in the same potential range as GITT.

### Unit cell volume changes before and after cycling

To investigate the stability of unit cells for LCP or LCTP composite with and without FP-coating, unit cell volume changes were calculated based on the *ex situ* XRD pattern before and after 50 cycles (Figure S9). As shown in Table S1, the volume of unit cells for coated samples remained constant after 50 cycles, while the value for uncoated samples increases. These results support other results shown in the main manuscript, all indicating the high stability of FP-coated samples. The increase in unit cell volume suggests the cation mixing in uncoated LCP or LCTP crystals, accompanied by the decay of crystal structure as reported<sup>1-2</sup> and confirmed by TEM images of samples after cycling (see Figure 4 in the main manuscript).

To better understand the phase formation during lithiation/delithiation in LCP-derived materials, we have additionally performed the dQ/dV analysis as shown in Figure S10. For all the three samples, the dQ/dV peak intensity largely diminished from 2<sup>nd</sup> to 100<sup>th</sup> cycle. Among three samples, however, only the FP-coated LCTP sample maintains the integrated peak area at 100<sup>th</sup> cycle as identical as that at 2<sup>nd</sup> cycle, indicating that the lithiation/delithiation for the FP-coated LCTP/MWCNT proceed smoothly even after 100 cycling. It should be noted that the widened peak potential separation did not affect the lithiation/delithiation at a slow C-rate of 0.2 C, but may affect them at faster C-rate of 1C as shown in Figure 1.

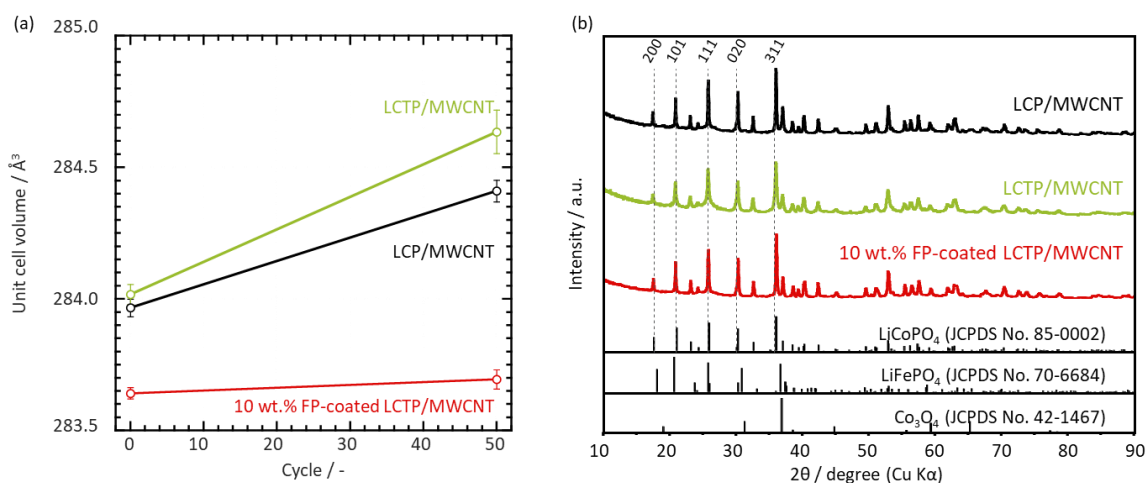


Figure S9 (a) Unit cell volumes of four different samples after charge and discharge up to 50 cycles; LCP, LCTP, and FP-coated LCTP/MWCNT composites. Each unit cell volume was calculated from the cell parameters obtained from corresponding (b) XRD-pattern analysis.

Table S1 Calculated cell parameters and unit cell volumes from XRD patterns of pristine and 50<sup>th</sup> cycled samples for LCP, LCTP, and FP-coated LCTP/MWCNT composites.

Sample	Cycle No.	$a / \text{\AA}$	$b / \text{\AA}$	$c / \text{\AA}$	$V / \text{\AA}^3$	$R_{wp}$	$R_p$	$R_e$	$S$	$\chi^2$
LCP / MWCNT	Pristine	10.2023(7)	5.9219(4)	4.7001(3)	283.97(3)	5.89	4.36	3.21	1.83	3.36
	50 <sup>th</sup>	10.2094(8)	5.9225(5)	4.7037(4)	284.41(4)	5.38	4.18	5.08	1.06	1.11
LCTP / MWCNT	Pristine	10.1972(8)	5.9229(4)	4.7025(4)	284.02(4)	4.09	3.00	2.90	1.41	1.98
	50 <sup>th</sup>	10.204(1)	5.922(1)	4.7100(8)	284.63(8)	5.30	4.10	5.02	1.05	1.11
10 wt.% FP-coated LCTP/MWCNT	Pristine	10.1877(4)	5.9192(3)	4.7036(2)	283.64(2)	4.73	3.43	2.89	1.64	2.68
	50 <sup>th</sup>	10.1794(7)	5.9167(4)	4.7103(4)	283.69(4)	5.55	4.30	5.02	1.11	1.22

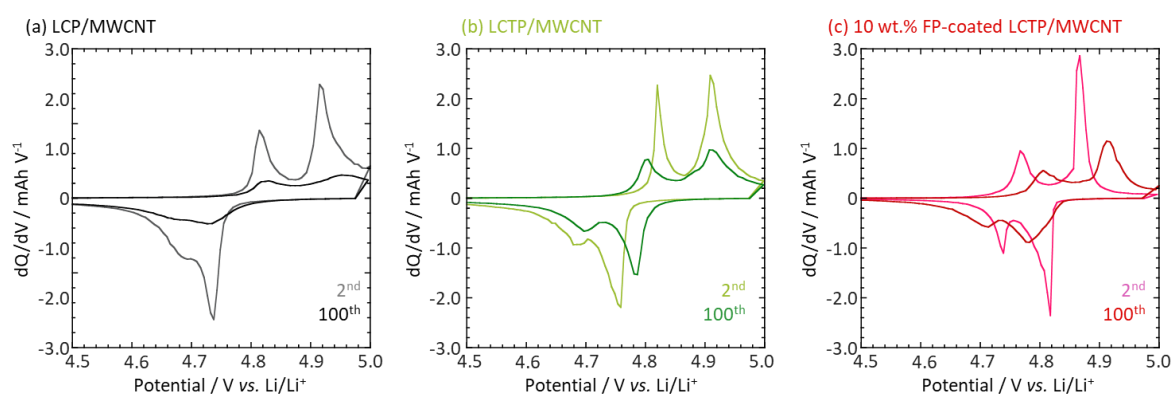


Figure S10  $dQ/dV$  plots for (a) LCP, (b) LCTP, and (c) FP coated LCTP/MWCNT cathodes in 1 M  $\text{LiPF}_6$  in EC:PC:DMC (1:1:3 in vol.) operated at CC-CV charge (0.2C-rate) and CC discharge (0.2C-rate) from Figure 1.

## References

- Okita, N.; Kisu, K.; Iwama, E.; Sakai, Y.; Lim, Y.; Takami, Y.; Sougrati, M. T.; Brousse, T.; Rozier, P.; Simon, P.; Naoi, W.; Naoi, K., Stabilizing the Structure of  $\text{LiCoPO}_4$  Nanocrystals via Addition of  $\text{Fe}^{3+}$ : Formation of  $\text{Fe}^{3+}$  Surface Layer, Creation of Diffusion-Enhancing Vacancies, and Enabling High-Voltage Battery Operation. *Chem. Mater.* **2018**, *30* (19), 6675-6683.
- Okita, N.; Iwama, E.; Takami, Y.; Abo, S.; Naoi, W.; Reid, M. T. H.; Naoi, K., Crystal-structure-matched  $\text{FePO}_4$  Surface-coating on  $\text{LiCoPO}_4/\text{MWCNT}$  Nanocomposites for Long Lifecycle 5 V Class Lithium Ion Batteries. *Electrochemistry* **2019**, *87* (3), 156-161.